An engineered POSS drug delivery system for copper(II) anticancer metallodrugs in selective application toward melanoma cells

Citation for published version (APA):
Guimarães Vieira, E., Enoque Ferraz de Paiva, R., Bernardi Miguela, R., de Oliveira, A. P. A., de Melo Bagatelli, F. F., Columbano Oliveira, C., Tuna, F., & da Costa Ferreira, A. M. (in press). An engineered POSS drug delivery system for copper(II) anticancer metallodrugs in selective application toward melanoma cells. *Dalton Transactions*.

Published in:
Dalton Transactions

OPEN ACCESS

ARTICLE

An engineered POSS drug delivery system for copper(II) anticancer metallodrugs in selective application toward melanoma cells

Eduardo Guimarães Vieira[a,c], Raphael Enoque Ferraz de Paiva[a], Rodrigo Bernardi Miguel[a], Ana Paula A. de Oliveira[a], Felipe Franco de Melo Bagatelli[b], Carla Columbano Oliveira[b], Floriana Tuna[c], and Ana Maria da Costa Ferreira*[a]

Abstract -

In this work, a polyhedral silsesquioxane (POSS) was used as an engineered drug delivery system for two oxindolimine-copper(II) anticancer complexes, [Cu(isaepy)]$^+$ and [Cu(isapn)]$^+$. The interest in hybrid POSS comes from the necessity of developing materials that can act as adjuvant to improve the cytotoxicity of non-soluble metallodrugs. Functionalization of POSS with a triazole ligand (POSS-atzac) permitted the anchorage of such copper complexes, producing hybrid materials with efficient cytotoxic effects. Structural and morphological characterization of these copper-POSS systems were performed by using different techniques (IR, NMR, thermogravimetric analysis). A combination of continuous-wave (CW) and pulsed EPR (HYSCORE) spectroscopies conducted at X-band have enabled the complete characterization of the coordination environment of the copper ion in the POSS-atzac matrix. Additionally, the cytotoxic effects of the loaded materials, [Cu(isapn)]@POSS-atzac and [Cu(isaepy)]@POSS-atzac, were assessed toward melanomas (SK-MEL), in comparison to non-tumorigenic cells (Fibroblast P4). Evaluation of their nuclease activity or ability to cleavage DNA indicated concentrations as low as 0.6 μg/mL, while complete DNA fragmentation was observed at 25 μg/mL. By using adequate scavengers, investigations on active intermediates responsible for their cytotoxicity were performed, both in the absence and in the presence of ascorbate as a reducing agent. Based on the observed selective cytotoxicity of these materials toward melanomas, investigations on the reactivity of complexes and corresponding POSS-materials with melanin, a molecule that contributes to melanoma resistance to chemotherapy, was carried out. Results indicated a main role of binuclear copper species, formed at the surface of the silica matrix, in the observed reactivity and selectivity.

[a.] *Departamento de Química Fundamental, Instituto de Química, Universidade de São Paulo. Av. Prof. Lineu Prestes 748, 05508-000 São Paulo, SP, Brazil;*
[b.] *. Departamento de Bioquímica, Instituto de Química, Universidade de São Paulo. Av. Prof. Lineu Prestes 748, 05508-000 São Paulo, SP, Brazil;*
[c.] *EPSRC National EPR Facility, Department of Chemistry and Photon Science Institute, University of Manchester, Oxford Road, M13 9PL, Manchester, UK..*

All

1. Introduction

The skin is the largest organ in the body, offering protection as a physical barrier [1]. Melanocytes are specialized cells in human skin that are responsible for synthesizing melanin inside melanosomes via a tyrosinase-dependent pathway [2]. Melanin is an ubiquitous pigment, formed by heterogeneous polyphenol-like biopolymers, responsible for the color of our skin, eyes, and hair [3, 4]. Its syntheses is initiated by tyrosine hydroxylation or *L-dopa* (L-3,4-dihydroxyphenylalanine) oxidation promoted by tyrosinase, a copper protein exhibiting in its active site a binuclear copper-histidine species, coordinated to dioxygen [5, 6]. Melanogenesis is stimulated by exposure of the skin to ultraviolet light [7], as a response to provide photoprotection against radiation damage. UV light exposure and genetic traits represent the main factors associated with melanocyte disorders, including melanoma development [8-10].

Melanoma is the second most prevalent type of skin cancer registered worldwide (324,635 cases in 2020), according to the Global Cancer Observatory, GCO – WHO [11]), and it has a mortality rate of 17.5%. Surgery is the primary treatment for all stages of melanoma [12], but chemotherapy is an important tool for managing the disease in its advanced form. The development of specific drugs for the treatment of melanoma only took off in the past 10 years, and metallodrugs have an important role, with the combination of carboplatin with paclitaxel as one of the possible therapeutic interventions [13].

In this context, the search for new anticancer compounds with diverse mechanisms of action becomes important to improve efficacy and circumvent resistance. In this study, two copper(II) compounds previously studied, [Cu(isapn)]$^+$ and [Cu(isaepy)]$^+$ [14] (Fig. 1B), have their anticancer activities explored against melanoma cells (SK-MEL-147). These compounds have been extensively investigated, and identified as promising antitumoral agents against different types of cancer in our group [15–17]. In the

recent advanced development of metallodrugs beyond the traditional and already approved platinum complexes [18], copper compounds have deserved a special interest among other stimuli-responsive metal complexes [19]. Besides having redox activity that improves its cytotoxicity versus tumour cells, copper centres are often coordinated to biologically active ligands as imines, triazoles or dithiocarbamates [20,21] that stabilize its oxidation states, frequently acting also as antioxidants or inhibitors of selected proteins in a synergistic effect [22, 23]. An useful strategy to modify and improve the cytotoxicity of metal complexes is loading them in inorganic nanoporous materials that can contribute significantly to its biological activities [24–26].

Among several suitable materials for engineered delivery system, the polyhedral oligomeric silsesquioxanes (POSSs) are the most important members of this kind of family owing to its non-toxicity, shape persistence, good biocompatibility, longer degradation time, and inert nature that make them highly attractive compared to polymers and surfactants for potential biomedical applications [27, 28]. In addition, octahedral POSS (RSiO$_{1.5}$)n (n = 8) are the smallest and precisely defined silica nanoplatforms (1-3 nm) with one to eight reactive organofunctional groups (R) attached to its eight possible vertices [29-31].

Furthermore, the main reasons for the use of nanocarriers in a drug delivery system is to decrease the high dosage used for free drugs to reach the designated targets, controlling the release of the active compound [32]. Therefore, an engineered drug delivery system based on POSS for tumorous cells has been attracting much attention nowadays since most of the anti-cancer drugs cause serious side effects on healthy cells [33].

Triazoles have attracted much attention since they represent a scaffold that appears in many commercial drugs, acting as antiviral, antibiotics, antifungal or anticancer agents [34–37]. They form metal complexes with different ions that usually show better biological

activity than their corresponding ligands [38]. In particular, the 3-amino-1,2,4-triazole-5- carboxylic acid ligand (atzac) used in this work to modify the surface of the precursor material (POSS-Cl) has been reported as an efficient ligand for copper ion. This ligand can form mononuclear, binuclear, and even mixed-valence Cu(I/II), or heterometallic as Cu(I)/Fe(II) coordination metal compounds [38]. In the atzac modification, the electron-rich N atoms of the triazole ring are available for coordination in addition to the oxygen atoms from carboxylic group. Therefore, this ligand seems to be suitable for functionalization of the silica.

Some studies in the literature have reported the use of different POSS for biological applications, however, none of them deal with the use of a modified POSS as a metallodrug carrier against tumor cells. Examples of organic drugs inserted on POSS include a synthesized hydrophilic polyhedral oligomeric silsesquioxanes [POSS(OH)$_{32}$] as a carrier for anthracyclines-doxorubicin (DOX) and daunorubicin (DAU) towards HeLa (cervical cancer endothelial) and MCF-7 (human breast adenocarcinoma) cell lines [39]. Furthermore, the biocompatibility *in vitro* of two water-soluble POSS-(SB)$_8$ and POSS-(QAS)$_8$ macromolecules were tested using mouse embryos osteoblast precursor cells (MC3T3-E1) treated for 24 h [40]. The cell viability results (> 80%) demonstrated a good biocompatibility and usability of each compound up to 500 μg/mL [40]. In other study, a modified POSS was applied in photodynamic therapy (PDT) [41]. According to the authors, *in vivo* imaging-guided photodynamic therapy has been successfully performed, and the material has shown no or negligible cytotoxicity. These results make POSS potentially eligible as a theranostic agent for PDT in clinical applications.

Herein an engineered drug delivery system was developed based on an hexa-triazole-substituted polyhedral oligomeric silsesquioxane (Figure 1A) as a carrier of two copper(II) metallodrugs whose cytotoxicity has been already verified toward different tumor cells (Figure 1B) [15, 42]. The loaded and free copper compounds were studied against the melanoma cell lines SK-MEL-147 and SK-MEL-05. To the best of our

knowledge, this is the first report on POSS materials as carriers for modified delivery of metallodrugs.
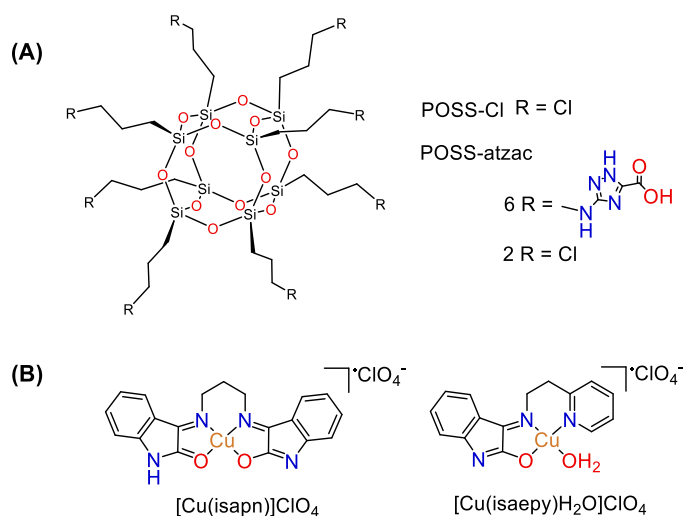

Figure 1. Molecular structure of (A) POSS-atzac, and (B) [Cu(isapn)]ClO$_4$ and [Cu(isaepy)H$_2$O]ClO$_4$.

The elucidation of the chemical environment of these copper(II) complexes upon loading on the POSS-atzac was provided recently by spectroscopic approach, combining continuous wave and pulsed wave EPR (HYSCORE) [43], indicating the formation of a secondary species capable to explain the better selectivity verified toward melanomas.

2. Experimental section

The chemicals 3-amino-1,2,4-triazole-5-carboxylic acid *(atzac)*, isatin (2,3-dioxoindole) *(isa)*, 2-(2-aminoethyl)pyridine *(epy)*, 1,3-diaminopropane *(pn)*, and copper(II) perchlorate hexahydrate, were purchased and used as received from Sigma-Aldrich/Merck.

2.1 Instrumentation

^{13}C and ^{29}Si CP/MAS NMR spectra were registered with a Bruker Avance 500 spectrometer with MAS@10kHz, at Institute of Chemistry of UNESP/Araraquara, SP. Infrared spectra, elemental and metal analyses were carried out by using Perkin Elmer – Frontier, CHN-Perkin Elmer-2400 and ICP-OES, Spectro Arcos instruments, respectively, at Central Analítica of IQ-USP, University of São Paulo/Brazil

(https://ca2.iq.usp.br/). Scanning electron microscopy (SEM) images were obtained using a Jeol – JSM 7401F (FEG) instrument. Continuous-wave (CW) EPR data were recorded with a Bruker EMX 300 EPR spectrometer operating at X-band (9.4 GHz, 20 mW power, 100 kHz frequency amplitude), at University of São Paulo (USP). The magnetic field was calibrated using DPPH as a standard (g = 2.0036). X-band pulsed EPR measurements have been performed at 5 K with a Bruker ElexSys E580X spectrometer operating at X-band (ca. 9.67 GHz), at University of Manchester, UK. The measurements at low temperature were accomplished with a helium cryostat from Oxford instruments for CW mode, and a Bruker ER4118HV-CF58 FlexLine Cryogen-Free System was used for pulse measurements. The magnetic field was calibrated using DPPH or Strong Pitch standards. The 2D FFT-HYSCORE experiments were obtained from baseline corrected with a hamming window and zero filled. EasySpin in combination with MATLAB 2015a platform (MathWorks) were used to perform the simulations, both for CW- and HYSCORE spectra [44].

2.2 Syntheses

2.2.1 Synthesis of the copper(II) complexes [Cu(isapn)]ClO₄ and [Cu(isaepy)(H₂O)]ClO₄

Syntheses of [N,N'[bis-(3,3'-indolin-2-one)]-1,3-diiminopropane]-copper(II) perchlorate ([Cu(isapn)]ClO₄) and aqua[N-[bis-(3-indolin-2-one)]-2-iminoethylpyridine]-copper(II) perchlorate ([Cu(isaepy)(H₂O)]ClO₄) complexes

Compounds [Cu(isapn)]ClO₄ (**1**) [14, 45] and [Cu(isaepy)(H₂O)]ClO₄ (**2**) were obtained following methods previously described by us [16]. Briefly, the imine ligand is obtained by condensation reaction of isatin with the suitable amine or diamine at pH around 6, followed by metalation with perchlorate salt.

[Cu(isapn)]ClO₄ · 2H₂O **1** ($C_{19}H_{19}N_4O_8ClCu$, 530.38 g/mol): Yield 85%, Calculated: C 43.03, H 3.80, N 10.56 %; Found: C 43.37, H 3.37, N 10.67%. FTIR (KBr pellet, cm⁻¹): ν(C=O) 1728, ν(C=N) 1595, and ν(C-H) 738.

[Cu(isaepy)(H₂O)]ClO₄ · 2H₂O **2** ($C_{15}H_{19}N_3O_8ClCu$, 468.33 g/mol): Yield 75%, Calculated: C 38.47, H 4.09, N 8.97 %; Found: C 38.96, H 3.98, N 8.93%. FTIR (KBr pellet, cm⁻¹): ν(C=O) 1731, ν(C=N) 1583, and ν(C-H) 744.

2.2.2 Synthesis of hexa[(3-amino-1,2,4-triazole-5-carboxylic acid) dichloropropyl] octasilsesquioxane (POSS-atzac)

The synthesis of precursor octakis(3-chloropropyl) octasilsesquioxane (POSS-Cl) **3** has been reported in previous work [30, 46]. Similarly, preparation of octa[3-amino-1,2,4-triazole-5-carboxylic acid) propyl] silsesquioxane (POSS-atzac) was firstly reported in our previous study [47]. However, a new synthesis of the POSS-atzac was performed again with modification in order to obtain a compound with six units of the 3-amino-1,2,4-triazole-5-carboxylic acid ligand bonded to the POSS-Cl surface.

POSS-Cl (5 g, 4.82 mmol) was added into two reaction flasks containing 100 mL dimethylformamide, and stirred under reflux until its complete solubilization. Next, the ligand 3-amino-1,2,4-triazole-5-carboxylic acid *(atzac)* (3.66 g, 28.92mmol) was added slowly into each flask over a period of 3 h and stirred for 3 more days. At the end of the reaction time, the solid was obtained after the addition of ethanol to the medium to precipitate the materials hexa[3-amino-1,2,4-triazole-5-carboxylic acid) dichloropropyl] octasilsesquioxane (POSS-atzac, white solid). The solid was separated by filtration and washed with a mixture of ethanol/H₂O (50:50 v/v).

POSS-Cl [$Si_8O_{12}(C_3H_6Cl)_8$] 1036.94 g/mol: Yield 49%, CHN (%), calculated: C 27.80, H 4.67; found: C 27.79, H 4.41. FTIR (KBr pellet, cm⁻¹): ν(C-H) 2954, ν(C-H) 1430, ν_{as}(Si-O-Si) 1110 and ν(C-Cl) 699.

POSS-atzac [$Si_8O_{12}(C_6H_9N_4O_2)_6(C_3H_6Cl)_2$].$(H_2O)_{23}$.$(HCl)_6$ 2219.81 g/mol: Yield 95%, CHN (%), calculated: C 22.73, H 5.36, N 15.14; found: C 22.62, H 5.05, N 14.90. FTIR (KBr pellet, cm⁻¹): ν(C-H) 2942, ν(C=O) 1674, ν(C=N) 1574, ν(C-N) 1449, ν_{as}(Si-O-Si) 1114 and ν(C-Cl) 696.

2.2.3. Synthesis of binuclear complex [Cu(isapn)(μ-triazole)Cu(isapn)]

The synthesis of the binuclear complex was carried out by solubilizing the 3-amino-1,2,4-triazole-5-carboxylic acid ligand (2.25 mmol) in hot water. Then, the [Cu(isapn)]ClO4 complex (6.2 mmol) solubilized in DMSO/H2O (20:80) v.v at pH 7 was added to the reaction medium and left under stirring for 2h. Next, binuclear complex [Cu(isapn)(μ-triazole)Cu(isapn)] was filtrated and washed several times with a mixture of DMSO/H2O. The sample was dried at 70°C overnight and stored in glass flasks.

[Cu(isapn)(μ-triazole)Cu(isapn)] C41H36Cu2N12O6 918.15 g/mol: Yield 94%, Calculated (%) C 53.53, H 3.94, N 18.27, Cu 13.82; Found (%): C 53.39, H 3.88, N 18.16, Cu 13.75.

2.2.4 Loading of copper compounds on POSS: [Cu(isapn)]@POSS-atzac and [Cu(isaepy)]@POSS-atzac

Both copper complexes loaded on POSS were obtained following a similar method. Either [Cu(isapn)]+ or [Cu(isaepy)]+ (4.5 mmol) were solubilized in DMSO/H2O (2:8 v/v) at apparent pH 6.4. Next, 2.25 mmol of POSS-atzac (5 g) were slowly added over a period of 2h under stirring. The resulting suspension was stirred for 20 h at room temperature. The materials [Cu(isapn)]@POSS-atzac and [Cu(isaepy)]@POSS-atzac were isolated as solids by filtration and washed exhaustively with a mixture of DMSO/H2O 2:8. The samples were dried at 70°C overnight, ground with mortar and pestle and stored in amber glass flasks.

[Cu(isapn)]@POSS-atzac
{[$Si_8O_{12}(C_6H_9N_4O_2)_6(C_3H_6Cl)_2$].($H_2O$)$_{20}$.(HCl)$_6$}$_2$[Cu($C_{19}H_{15}N_4O_2$)]ClO$_4$ 4825.87 g/mol: Yield 96%, Calculated (%) C 25.64, H 4.99, N 15.09, Cu 1.32; Found (%): C 25.19, H 4.01, N 15.56, Cu 1.02. FTIR (KBr pellet, cm^{-1}): ν(C-H) 2935, ν(C=O) 1656, ν(C=N) 1568, ν(C-N) 1454, ν$_{as}$(Si-O-Si) 1111, and ν(C-Cl) 703.

[Cu(isaepy)]@POSS-atzac
{[$Si_8O_{12}(C_6H_9N_4O_2)_6(C_3H_6Cl)_2$].($H_2O$)$_{20}$.(HCl)$_4$}$_2$[Cu($C_{15}H_{15}N_3O_2$)]ClO$_4$ 4617.99 g/mol: Yield 93%, Calculated (%): C

25.75, H 5.13, N 15.47, Cu 1.38; Found (%): C 25.64 H 5.19, N 15.25, Cu 1.39. FTIR (KBr pellet, cm^{-1}): ν(C-H) 2942, ν(C=O) 1670, ν(C=N) 1573, ν(C-N) 1460, ν$_{as}$(Si-O-Si) 1116 and ν(C-Cl) 699.

2.3 Release experiments

The release experiments were designed to simulate the same conditions used for cell experiments. In this experiment, 200 μL of the 0.5 mg/mL DMEM solutions of [Cu(isapn)]@POSS-atzac, and [Cu(isaepy)]@POSS-atzac were placed in a 96-well plate in triplicate. The plate was kept at 37 °C and at different 180 μL aliquots were collected over time for each compound and transferred to a microtube. The tubes were centrifuged at 14 000 rpm for 5 min, the supernatants were collected and the total copper content was determined by ICP-MS.

2.4 Cells and cell culture

SK-MEL-147 (wild type, Cellosaurus, CVCL 3876 - Human melanoma cells) and SK-MEL-05 were kindly provided by Professor Roger Chammas from the Cancer Institute of São Paulo State (ICESP, São Paulo). The human foreskin fibroblasts P4 cells (non-tumorigenic) were isolated from tissues at Faculty of Pharmaceutical Sciences-USP in the lab of Professor Silvya Stuchi Maria-Engler. Dulbecco's Modified Eagle's medium - DMEM (Vitrocell) supplemented with 10% fetal bovine serum – FBS (Vitrocell) was used to cultivate both cell lines in an oven with 5% CO2 atmosphere and 37°C.

2.4.1 Cell viability analysis

Cell viability was evaluated by the tetrazolium dye reduction assay (MTT) to verify the cytotoxicity of the free and attached complexes on two modified-POSS. 1.10^4 of melanoma and non-tumor cells (SK-MEL-147, SK-MEL-05 and fibroblast P4, respectively) were placed in a 96-well plate and growth for 24h. Next, the medium was removed, and each well was washed three times with phosphate buffered saline buffer (PBS), pH 7.4. The solutions and suspensions of each compound were prepared in culture medium and directly added to the cells and treated for 24 and 48h. Subsequently, the

medium was replaced by 200 µL of medium containing 0.2 mg/mL of 3-(4,5-dimethylthiazol-2-yl)-2,5-diphenyltetrazolium bromide reagent (MTT, Sigma Aldrich) and incubated for 3h. After the incubation, it was possible to detect the formation of formazan crystals under a microscope, after solubilization by addition of 100 µL DMSO. Final absorbance was measured at 570 nm on a microplate reader (Tecan Infinite M200, Switzerland) and the cytotoxicity was expressed as IC_{50} values, determined from the concentration-response curve.

2.5 Nuclease activity

2.5.1 Plasmid expression and purification

The plasmid pBlueScript II SK (+), from here on referred to as pBS, was used as a double strand DNA substrate (2961 bp-long) to evaluate the nuclease activity of the materials prepared in this study. It was expressed in *E. coli* (DH5a strain) cultivated in 5 ml LB-Ampicillin (50mg/ml) broth and purified to molecular biology grade using a QIAprep Spin Miniprep Kit (QIAGEN). Briefly, bacterial cells were pelleted in microcentrifuge tubes, resuspended in 250 µL of buffer P1 (composition: 50 mM Tris·Cl, 10 mM EDTA at pH 8.0 supplemented with 100 µg/ml RNase A) and lysed by addition of 250 µL of buffer P2 (200mM NaOH, 1% SDS) with thorough mixing. After quenching with 350 µL of neutralization buffer N3 (proprietary composition, QIAGEN) and centrifugation for 10 min at 13000 rpm, the supernatant obtained was carefully transferred by pipetting to a QIAprep 2.0 spin columns. The system was centrifuged for 1 min, the first flowthroughs were discarded and each column was washed with 0.75 mL buffer PE (proprietary composition, QIAGEN). Finally, the plasmid were collected by centrifugation (1 min), eluted with 50 µL elution buffer (10 mM Tris·Cl, pH 8.5) into clean microcentrifuge tubes, pooled and had the final concentration determined spectrophotometrically using a NanoDrop 2000 instrument (Thermo Fisher). The pBS purity and integrity were further confirmed by an agarose gel electrophoresis run before treatment with the compounds of interest.

2.5.2 Nuclease Activity in the absence of a reducing agent

The nuclease activity of [Cu(isapn)]@POSS-atzac and [Cu(isaepy)]@POSS-atzac was evaluated by agarose gel mobility shift. 200 ng of pBS were exposed to increasing concentrations of the materials in 1x PBS (10 mM phosphate, 137 mM NaCl, 2.7 mM KCl, pH 7.4) for 24h at 37 °C (20 µL total sample volume). After incubation, 4 µL of loading buffer were added to each microtube, homogenized, and 10 µL of each sample were loaded in a well of a 1% agarose gel containing ethidium bromide. Electrophoretic separation was run at 100V in 1x TAE buffer (in around 1 h), along with a control well loaded with 1kb plus DNA ladder (Thermo Fisher). The gels were photo documented in a UV chamber.

2.5.3 Nuclease Activity in the presence of ascorbate as a reducing agent

The formation of reactive oxygen species (ROS) induced by [Cu(isapn)]@POSS-atzac and [Cu(isaepy)]@POSS-atzac was probed in the presence of added ascorbate as a reducing agent. This experiment followed the same protocol described in section 2.4.3, but in the presence of added 1 mM ascorbic acid. With this experiment, we determined the minimum concentration of each compound where complete DNA fragmentation was observed, and the minimum concentration where at least single-strand formation (nicking) could be detected. Therefore, the concentrations were optimized in a per-compound basis.

2.5.4 Assignment of ROS species related to the nuclease activity

This experiment was carried out to identify the ROS families related to nuclease activity of materials [Cu(isapn)]@POSS-atzac and [Cu(isaepy)]@POSS-atzac. 200 ng of pBS were pre-mixed with 4 families of ROS scavengers: NaN_3 (500 mM; singlet oxygen); superoxide dismutase (40U; superoxide); dmso (10%; hydroxyl) and catalase (60U, peroxide). Next, an amount of each compound that was identified to cause complete DNA fragmentation in the presence of ascorbate (experiment described in 2.5.3) was then added to each

corresponding sample. Lastly, ascorbate was added for a final concentration of 1 mM, in 1x PBS and a total sample volume of 200 µL. The samples were incubated for 24 h at 37 °C, and 4 µL of loading buffer were added to each microtube. Gel run and photo documentation followed the same protocol given in 2.4.3.

2.6 Oxidative stress

To monitor the effect of the compounds on the redox state of SK-MEL-147, a flow cytometry assay was performed using the Muse Oxidative Stress Kit (MCH100111) (Merck Millipore). This assay simultaneously counts and determines the percentage live cells (ROS-) and cells undergoing oxidative stress (ROS+) based on the intracellular detection of superoxide radicals by the probe dihydroethidium (DHE). $1x10^5$ cells were seeded into each well of a 6-well plate containing 1 mL of DMEM culture medium supplemented with 10% SFB for 24 h at 37°C under 5% CO_2 atmosphere. After this treatment period, the cells were washed three times with PBS and a new DMEM culture medium was added containing each compound at their respective IC_{50} values, at 37 °C and atmosphere of 5% CO_2. The control group being maintained under the same conditions, however, in the absence of the compounds. After this period, the cells were re-suspended with trypsin-EDTA and transferred to an Eppendorf, then centrifuged at 300 g for 5 minutes. The supernatant was discarded, and the pellet was washed one time with the 1X buffer and centrifuged again at 300 g for 5 minutes. The supernatant was again discarded and 1X buffer pellet was added to the pellet until the solution remained at $1 \times 10^6 \times 1 \times 10^7$ cells/mL. Then, 10 µL of this cell suspension was collected and transferred to another Eppendorf where 190 µL of Muse Oxidative Stress Working Solution was added, which was previously diluted 1:8000 in the 1X buffer. The mixture was incubated for 30 min at 37 °C, and after this period, the Muse Cell analyzer was read.

2.7 Melanin oxidation assays

A microplate reader-compatible melanin oxidation assay was developed under physiological pH inspired by classical methods based on the detection of fluorescent oxidation product [48]. A 200 µg/mL stock solution of synthetic melanin was prepared in 1x PBS, pH 7.4. In a black walled 96-well plate, 100 µg/mL samples of melanin were then exposed to [Cu(isapn)]@POSS or [Cu(isaepy)]@POSS (final concentrations of 2.5 or 25 µg/mL) and the free compounds [Cu(isapn)]+ or [Cu(isaepy)]+ (final concentrations of 1 or 10 µM). Each compound was assayed in triplicate in PBS 1x pH 7.4, either in the absence or in the presence of 1 mM ascorbate, or 1.2 mM H_2O_2. Controls with free melanin, and melanin exposed to the same concentrations of ascorbate and H_2O_2 were also prepared, as well as the free matrix POSS-atzac (2.5 and 25 µg/mL) either in the absence or in the presence of ascorbate and H_2O_2. Further, a triplicate of 100 µg/mL melanin samples (250 µL) were incubated with 10% H_2O_2 for at least two hours. These samples were used to set the gain of the instrument. The bottom read of fluorescence ware taken over time (24h, 30 min cycles, 37 °C) with a microplate reader (Tecan Infinite M200, Switzerland) set with λ_{ex}= 470 nm and λ_{em}= 550 nm. The data were normalized to the maximum fluorescence reads.

3. Results and Discussion

3.1 Synthesis and characterization of POSS-atzac

The precursor material POSS-Cl was synthetized by acid hydrolytic condensation of the silylating agent 3-(Chloropropyl)triethoxysilane (CPTES) as previously reported [49]. Subsequent, POSS-Cl was modified stoichiometrically with a triazolic ligand, 3-amino-1,2,4-triazole-5-carboxylic acid *(atzac),* in a molar ratio of 1:6 so that a maximum of six units of each ligand were bound on the POSS surface. This stoichiometry was used, based in preliminary studies showing that the matrix with more than six units of ligands on its surface exhibited a high cytotoxicity, and no selectivity between tumor and non-tumorigenic cell lines. In contrast, the hybrid

material functionalized with six or less ligands showed a higher cytotoxicity toward melanoma tumor cells with high selectivity index. According to nitrogen elemental analysis of POSS-atzac, the degree of functionalization was 2.66 mmol of *atzac* groups per g of material, attesting that six units of 3-amino-1,2,4-triazole-5-carboxylic acid were linked to the POSS-Cl. Additionally, the existence of 3-amino-1,2,4-triazole-5-carboxylic acid ligand on POSS-Cl was certified by ^{13}C solid-state NMR spectroscopy (Figure 2).

POSS-atzac spectrum (Figure 2A) displays four peaks at 8.77 (CH_2-Si) (1), 22.62 (CH_2-CH_2Si) (2), 47.66 ppm (CH_2-N) (3) and 63.22 (CH_2-Cl) (4), which are allocated to the carbon of the propyl chain. However, a similar chemical environment can be seen among carbons 1/1* and 2/2* which reflects in the greater intensity of these signals. Additionally, it is observed a difference in the chemical displacement for carbons 3 and 4. Furthermore, four new peaks appear at 154.62 (5), 148.79 (6) and 139.55(7) derived from carbons of the aromatic ring, and the assigned 5* peak may be assigned to the deprotonation of -COOH group leading a change in the chemical environment of the carbon 5. The ^{29}Si NMR spectrum of POSS-atzac (Figure 2B) exhibits a single peak at -67.38 ppm; confirming that the core remains closed due to a single silicon environment.
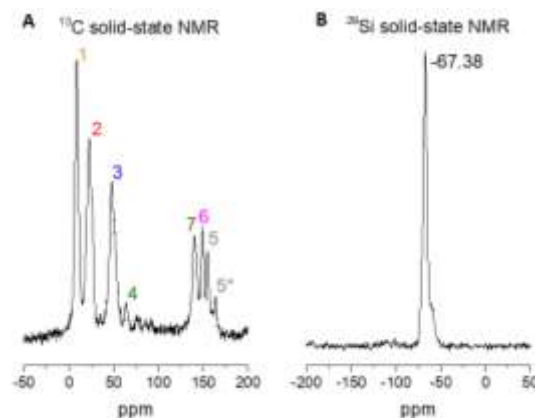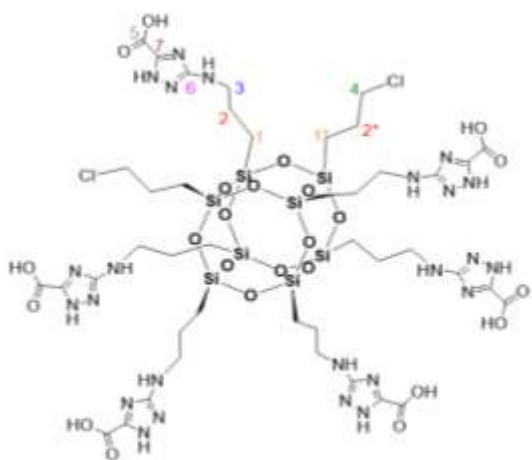

Figure 2. Structure, ^{13}C **(A)** and ^{29}Si **(B)** solid-state NMR spectra of the hexa[3-amino-1,2,4-triazole-5- carboxylic acid) chloropropyl] octasilsesquioxane (POSS-atzac).

3.2 Characterization of the loaded materials [Cu(isapn)]@POSS-atzac and [Cu(isaepy)]@POSS-atzac

Preliminary loading tests of [Cu(isapn)]$^+$ on POSS-atzac was performed and evaluated by EPR spectroscopy as can been seen in Figure S1A. The results showed that the loading of the [Cu(isapn)]$^+$ on the POSS-atzac matrix is a function of time (vide Figure. S1B), and the equilibrium condition was reached at 16 h of incubation at room temperature. From these preliminary data, it was also assumed that the maximum loading of [Cu(isaepy)]$^+$ complex on the POSS-atzac would be between 16 and 20 h of exposure.

Next, the oxindolimine-copper(II) complexes [Cu(isapn)]ClO$_4$ and [Cu(isaepy)(H$_2$O)]ClO$_4$ were loaded on POSS-atzac matrix and characterized by a range of techniques. Elemental analyses and ICP-OES data indicated the presence of 1 equivalent of [Cu(isapn)]ClO$_4$ or [Cu(isaepy)(H$_2$O)]ClO$_4$ for 2 equivalents of POSS-atzac. The morphology of each material was investigated by Scanning Electron Microscopy (MEV). At a magnification of 10,000x (Figure 3), it can be observed that the free matrix POSS-atzac (Figure 3, panel A) has clearly smaller grains than both loaded materials [Cu(isapn)]@POSS-atzac and [Cu(isaepy)]@POSS-atzac. Upon loading with [Cu(isapn)]$^+$ or [Cu(isaepy)]$^+$, differences in size became negligible (Figure 3, panels B and C). The magnifications

of 1,000x and 50,000x (Figure S2 and S3) display the same behavior.

As can be seen in Figure S4, the FTIR spectra of each material show strong and broad bands around 3500 cm^{-1}, assigned to OH-stretching of silanol groups along with adsorbed water. The intense band about 1100 cm^{-1} is typical of siloxane groups (Si-O-Si) present in each compound and in precursor material (POSS-Cl) [49,50]. Additionally, the bands νC-H nearby 2957 and 2877 cm^{-1} come from and it is due to the propyl chain of the precursor POSS-Cl, as shown in Figure S4A [50]. The presence of the bands of *atzac* ligand functionalized on POSS-Cl appear at 1674, 1574 and 1449 cm^{-1}, and at 2500, 1636, 1541, 1442 and 1250 cm^{-1} relative to the binding ν(C=O), ν(C=N) and ν(C-N) for POSS-atzac (Figure S4B), respectively [51, 52]. Since only six units of *atzac* ligand were inserted on functionalized POSS-Cl, the bands assigned to ν(C-Cl) remain in their structure at 696 cm^{-1}. On the other hand, the bands of pure copper(II) complexes (Figures S5A and S5B) attached/bonded on POSS-atzac are not clearly evident due to these bands appear in the same range as the functionalized *atzac* ligand. However, it is possible to observe slight band shifts in the spectra of metal-compound (Figures S4C and S4D) confirming the coordination of the complexes to the *atzac* group.
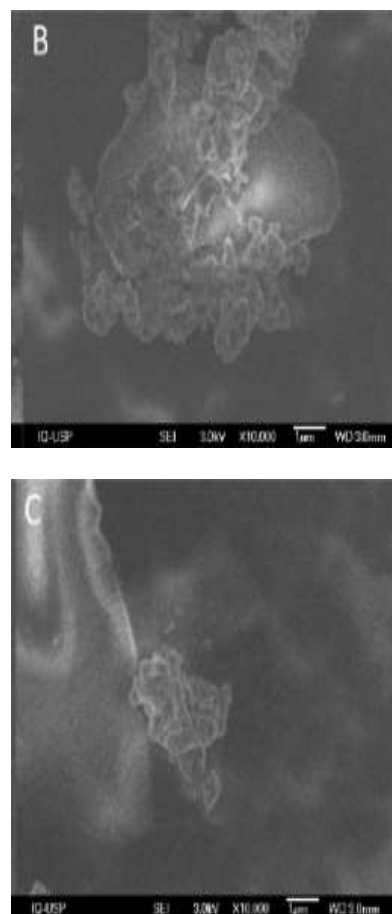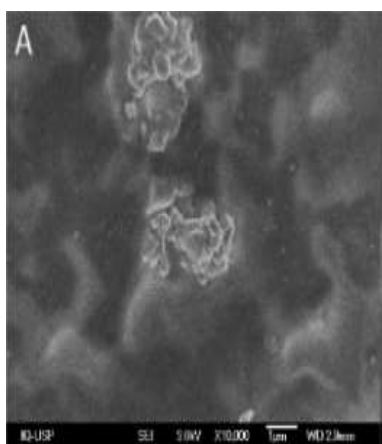

Figure 3. Scanning electron micrographs of materials **(A)** POSS-atzac, **(B)** [Cu(isapn)]@POSS-atzac and **(C)** [Cu(isaepy)]@POSS-atzac at 10,000x magnification.

The precursor material POSS-atzac along with the two metal-compounds were subjected to thermogravimetric analyses (TGA) to investigate their stability. All compounds due to their silsesquioxane core have shown to be thermally stable up to about 250 °C. As can be seen in Figure S6, in general all first mass loss occurs up to 100 ºC concerning the loss of physiosorbed water [53–56]. The second mass loss occurs in two steps. The first starts from 100 °C to 365 °C and the second step from 365°C to 946 °C attributed to the decomposition of the organic part that includes the chloro- and atzac-propyl chain for POSS-atzac. In addition, the combustion profiles of [Cu(isapn)]@POSS-atzac and [Cu(isaepy)]@POSS-atzac compounds also refer to losses of the chloro- and atzac-propyl chains along with *isapn* and *isaepy* ligands derived of complexes **1** and **2**, respectively.

Continuous-wave EPR spectroscopy was used to probe the environment of the copper(II) ions in the loaded materials, given Cu(II) has a $3d^9$ (s =1/2) configuration and is therefore paramagnetic. X-band EPR spectra at room temperature of [Cu(isapn)]@POSS-atzac and [Cu(isaepy)]@POSS-atzac materials are presented in Figure 4. These are dominated by the expected characteristics of the respective copper(II) complexes, confirming the successful loading and attachment to the POSS-atzac surface of both complexes. Best simulation of the spectra was achieved with the set of parameters presented in Table 1. Analysis of the data indicates that the copper coordination environment in all loaded materials is quite different from that found in free complexes as evidenced by g_{iso} values (Table 1). This may be due to tetra- and tri-coordinate complexes ([Cu(isapn)]$^+$ and [Cu(isaepy)$^+$, respectively) bond covalently to nitrogen or oxygen atoms on POSS-atzac. In contrast, previous studies in our lab using similar Schiff base copper(II) complexes inserted in smectite clays [57] showed g_{iso} values for free $(g_{iso}$ = 2.111$)$ and loaded complexes $(g_{iso}$ = 2.105$)$, that demonstrated a weak electrostatic interaction of copper compounds in the lamellae. Further, the [Cu(isapn)]$^+$ has been previously loaded in a modified-MCM matrix and the EPR parameters displayed were also distinct for the free $(g_{iso}$ = 2.180) and loaded complexes (g_{iso} = 2.151) [25].
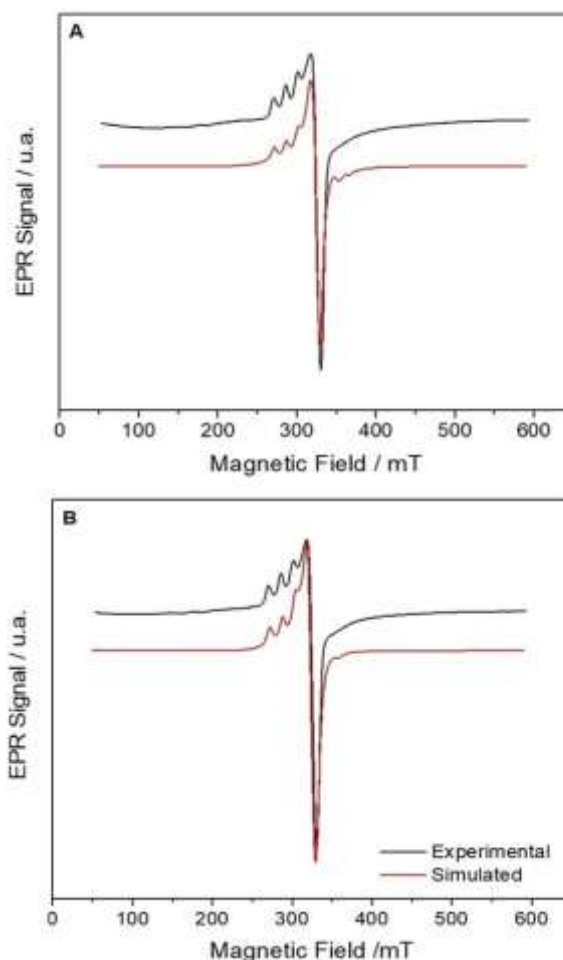
Figure 4. Experimental (black) and simulated (red) EPR spectra at X-band (9.4 GHz) and 298 K of solid state samples of (A) [Cu(isapn)]@POSS-atzac, and (B) [Cu(isaepy)]@POSS-atzac (B). Simulation parameters are displayed in Table 1.

To provide a conclusive evidence regarding the final coordination environment of the loaded material [Cu(isapn)]@POSS-atzac, HYSCORE experiments were previously conducted, as recently reported [43]. Results pointed to a major single symmetrical copper(II) species, containing a keto-keto or enol-enol form, surrounded by five nitrogen atoms, and the corresponding parameters were determined. *N1* and *N2* donor atoms from the di-imine group have a stronger coupling in comparison to non-coordinated *N3* and *N4* atoms from indole rings.

Completing the coordination sphere, *N5* can be assigned to one of the nitrogen atoms of the triazole moiety in the matrix, showing the weakest coupling

among the five nitrogen atoms. However, experiments also pointed to a minor binuclear species (see Figure 5) where the triazole moiety acts as a bridge between two copper centers, that can explain the selectivity toward melanoma cells [43, 58]. The preparation of a mimetic binuclear complex [Cu(isapn)(μ-triazole)Cu(isapn)] showing very similar EPR parameters attested this statement [43].
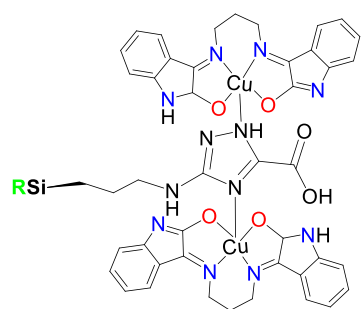
R = POSS-atzac-[Cu(isapn)]

Figure 5 – Proposed structure for the minor binuclear copper(II) species formed inside the POSS matrix.

the same period of time was around 15% (red line). Owing to a stronger interaction between [Cu(isapn)]⁺ complex and the POSS-atzac matrix, a positive careful release could be seen for [Cu(isapn)]@POSS-atzac to reach its target. The total released for [Cu(isapn)]@POSS-atzac material after 2 h was close to 25 %. In contrast, the copper release for [Cu(isaepy)]@POSS-atzac proved to be faster, reaching 85 % of total complex released after 2 h. Based on these data, the POSS-atzac studied here is a promising anticancer drug delivery system, as it has the necessary properties for the release of both complexes [Cu(isapn)]⁺ and [Cu(isaepy)]⁺ to their appropriate site of action.

Table 1. EPR parameters estimated through simulation for free [Cu(isapn)]⁺ and [Cu(isaepy)]⁺ complexes in frozen dmso solution at 77K, and loaded materials in solid-state at 298 K.

Compounds	Temp.	g_{iso}	$g_\perp$	$g_{//}$	$A_{//}$, G
[Cu(isapn)]ClO₄	77K	2.1800	2.1140	2.3110	118
[Cu(isaepy)H₂O]ClO₄	77K	2.1530	2.0750	2.3090	154
[Cu(isapn)]@POSS-atzac	298K	2.1346	2.0644	2.2751	148
[Cu(isaepy)]@POSS-atzac	298K	2.1363	2.0720	2.2651	154

3.3 Metallodrug release experiments

The release curves of both copper complexes [Cu(isapn)]⁺ and [Cu(isaepy)]⁺ loaded on POSS-atzac was studied in DMEM at 37 °C, under continuous stirring on a rocking table (dissolutor). Copper was determined by ICP-MS and the time-courses for the release of both compounds are shown in Figure 6. [Cu(isaepy)]⁺ (blue line) release reached released from POSS-atzac surface (~60%), during the first hour. On the other hand, the rate release of [Cu(isapn)]⁺ complex from POSS-atzac matrix within
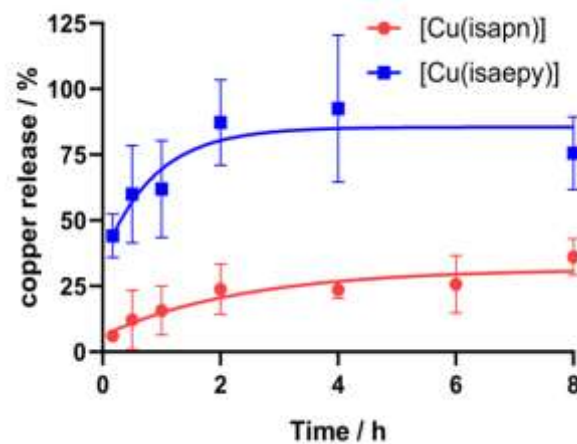
Figure 6. Release of copper from [Cu(isapn)]@POSS-atzac and [Cu(isaepy)]@POSS-atzac as determined by ICP-MS. Experiments were carried out in DMEM to simulate the conditions used for cellular experiments, at 37 °C with continuous shaking on a rocking table.

Similar mesoporous delivery systems have been reported in the literature [59] describing a molecularly imprinted polymer and the release of paclitaxel (PTX) by LC POSS NIPs (N3) that reached 100 % delivering in 6h. Maximum delivery in a short period of time may be related to the drug's polarity resulting in a weak interaction between the drug (organic or inorganic) and the carrier [60]. In contrast, a synthesized mesoporous silica nanoparticles with folic acid (FA) showed a different release profile reaching 30 % FA delivery in 72 h [61].

loaded complexes on modified-matrix: [Cu(isapn)]@POSS-atzac and [Cu(isaepy)]@POSS-atzac were evaluated toward the NRASQ61R mutated SK-MEL-147 cells [62] and compared to non-tumorigenic Fibroblast P4 cell line, by the tetrazolium dye reduction assay (MTT). Growth inhibition on SK-MEL-147 and Fibroblast P4 cells induced by the free copper(II) complexes and their loaded species on the POSS-atzac surface are shown in Figures S8-S10, at either 24 or 48h exposure times.

Table 2: Results of the antiproliferative assay determined by MTT assay of the two modified-POSS matrices used, and of loaded complexes on them, toward tumor and non-tumor cell lines. IC_{50} values for the free and loaded matrices (as a single compound) are expressed in µg/mL and the corresponding values in µmol/L (considering 100% of complexes delivered) are given in parentheses.

Material	SK-MEL-147		Fibroblast P4	
	24h	48h	24h	48h
POSS-Cl	> 500 (> 482)	> 500 (> 482)	> 500 (> 482)	> 500 (> 482)
POSS-atzac	161 ± 10 (73)	141 ± 5 (64)	> 500 (> 225)	> 500 (> 225)
		'		
[Cu(isapn)]@POSS-atzac	111 ± 4 (23)	49 ± 3 (10)	336 ± 5 (71)	267 ± 7 (56)
[Cu(isaepy)]@POSS-atzac	93 ± 2 (20)	62 ± 2 (13)	197 ± 6 (43)	111 ± 5 (24)

However, despite the differences observed between [Cu(isapn)]@POSS-atzac and [Cu(isaepy)]@POSS-atzac release profiles, the cytotoxicity values *(IC$_{50}$)* of both loaded compounds are close, and present a remarkable improvement in relation to the free complexes, mainly in relation to the [Cu(isapn)]$^+$ complex.

3.4 Antiproliferative activity

Cell viability of the free complexes: [Cuisapn)]ClO$_4$; [Cu(isaepy)H$_2$O]ClO$_4$; non-functionalized matrix: POSS-Cl; functionalized matrix POSS-atzac; and

As can be seen in Table 2, the matrix POSS-Cl presents little (> 500 µM) or no toxicities toward SK-MEL-147 and fibroblast P4 cell lines. The functionalized matrix POSS-atzac exhibits a greater cytotoxicity against SK-MEL-147 in comparison to POSS-Cl; however, it does not lead to an observed increase in cytotoxicity against Fibroblast cells line. This can indicate that the triazole ligand *(atzac)* have some effect on toxicity toward SK-MEL-147 cells. In addition, POSS-atzac has equivalent cytotoxicities after 24 and 48h incubation toward these cells. A

clear selectivity between tumor and non-tumor cell lines for POSS-atzac has already been observed.

In general, the matrices loaded with a metal complex display a significant increase in cytotoxicity for both studied cell lines in 24 h of exposure, and the selectivity between tumor and non-tumor cells was maintained. In 48 h of treatment, the materials [Cu(isapn)]@POSS-atzac and [Cu(isaepy)]@POSS-atzac show IC_{50} values of 10 and 13 μM respectively against SK-MEL-147, becoming twice as much cytotoxic compared to 24 h.

Table 3 shows that although a low amount of either [Cu(isapn)]$^+$ or [Cu(isaepy)]$^+$ was loaded on the POSS-atzac, these materials still exhibit a higher cytotoxicity as indicated by the IC_{50} values expressed in terms of the relative amount of complex in each material. For comparison, the determined IC_{50} value for the binuclear complex [Cu(isapn)(μ-triazole)Cu(isapn)], around 80 μM, was lower than for the analogous mononuclear, [Cu(isapn)]ClO$_4$ (> 100 μM), as expected.

works by one-electron transfer reactions, while the binuclear ones can act by two-electron transfers, in analogy with tirosinase activity [5, 6]. This comparison, along with the cytotoxic data presented here, highlights the success of the strategy of combining a copper compound with the POSS-atzac as a matrix to increase the cytotoxicity and selectivity of the copper metallodrug.

3.5 Nuclease Activity Assays

To start probing potential biological applications of the materials developed in this study, the oxidative cleavage of plasmid DNA (Bluescript) was explored. The nuclease activity of the loaded materials [Cu(isapn)]@POSS-atzac and [Cu(isaepy)]@POSS-atzac was probed either in the absence and in the presence of ascorbate (Figure 7).

Table 3: Estimated IC_{50} (μM) values expressed in terms of the relative amount of each complex in the POSS-atzac matrix, considering the experimentally determined release of 25% and 85% for [Cu(isapn)]@POSS-atzac and [Cu(isaepy)]@POSS-atzac, respectively, based on ICP-MS data.

Compound	SK-MEL-147		Fibroblast P4	
	24h	48h	24h	48h
[Cu(isapn)]ClO$_4$	> 100	> 100	> 100	> 100
[Cu(isaepy)H$_2$O]ClO$_4$	38 ± 4	12 ± 3	51 ± 2	23 ± 2
[Cu(isapn)(μ-triazole)Cu(isapn)]	80 ± 2		> 100	
[Cu(isapn)]@POSS-atzac	0.63 ± 0.02	0.27 ± 0.02	1.95 ± 0.03	1.54 ± 0.04
[Cu(isaepy)]@POSS-atzac	1.72 ± 0.04	1.12 ± 0.04	3.71 ± 0.11	2.07 ± 0.09

Comparatively, a binuclear similar copper(II) compound containing imine ligands was found to have an IC_{50} value of 20.0 ± 7.0 μM vs. SKMEL-147 [63]. Also in this case, a better efficiency against melanoma cell was verified with the binuclear species regarding the analogous mononuclear species [58, 63]. Possibly, the mode of action of such copper complexes are also modulated by its nuclearity. The mononuclear species
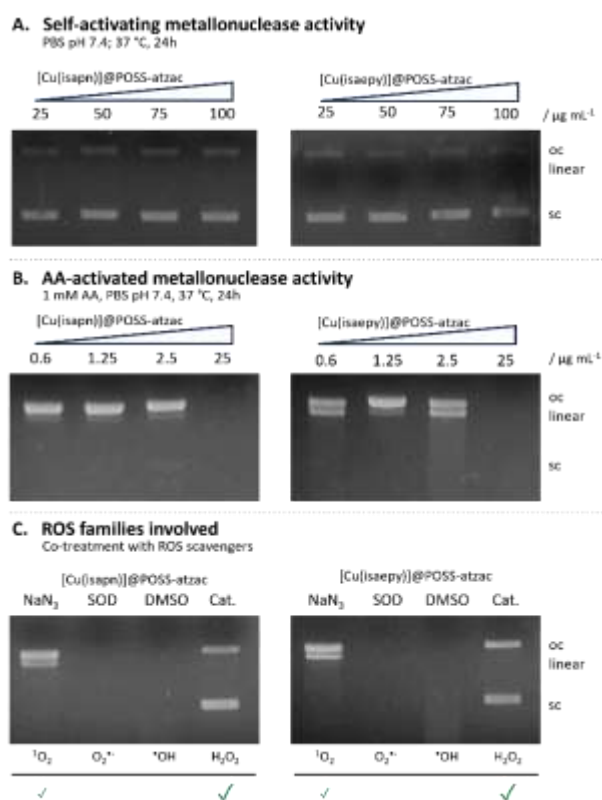
Figure 7. Nuclease activity assay of the loaded materials [Cu(isapn)]@POSS-atzac and [Cu(isaepy)]@POSS-atzac probed in the absence and in the presence of ascorbate. **(A)** In the ascorbate-free experiment, 200 ng of pBluescript (Bluescript plasmid) were exposed to concentrations of the compounds ranging from 25 to 100 µg mL^{-1} in 1x PBS buffer (10 mM phosphate, 137 mM NaCl, 2.7 mM KCl, pH 7.4) at 37 °C for 24 h. **(B)** In the ascorbate-activated experiment, 200 ng of pBluescript were exposed to the compounds in concentrations ranging from 0.6 to 25 µg mL^{-1} in the presence of 1 mM ascorbate in 1x PBS buffer at 37 °C for 24 h. **(C)** ROS tied to the nuclease activity of each material was identified in the presence of scavengers. NaN$_3$ was used as singlet oxygen ($^1O_2$) scavenger, superoxide dismutase (SOD) as superoxide ($O_2^{\bullet-}$) scavenger, DMSO as an HO$^\bullet$ scavenger and finally catalase was used as a H$_2$O$_2$ scavenger. Plasmid DNA forms: *sc*, supercoiled; *oc*, open circular; *linear*.

Figure 7A shows that the loaded materials [Cu(isapn)]@POSS-atzac and [Cu(isaepy)]@POSS-atzac had no prominent nuclease activity in the absence of ascorbate. On the other hand, in the ascorbate-activated experiment (Figure 7B), both materials lead

to complete DNA fragmentation at 25 µg/mL. The effect observed for [Cu(isaepy)]@POSS-atzac seems to be somewhat more prominent, based on the smearing clearly present at 2.5 µg/mL. The free matrix POSS-atzac has no nuclease effect, either in the absence or in the presence of ascorbate (Figure S11).

Furthermore, the reactive oxygen species (ROS) responsible for the AA-activated nuclease activity of both loaded materials were assigned (Figure 7C). In this experiment, pBS was exposed to a concentration of the loaded materials that led to total DNA fragmentation in the presence of ascorbate (25 µg/mL, as determined in the experiment shown in Figure 7B, but in the presence of four different ROS scavengers. [Cu(isapn)]@POSS-atzac and [Cu(isaepy)]@POSS-atzac induced reduced DNA fragmentation in the presence of catalase (DNA present in supercoiled and open circular form; major effect) and NaN$_3$ (DNA in open circular e linear form). This observation indicates that H$_2$O$_2$ and singlet oxygen ($^1O_2$) participate in the mechanism of ascorbate-activated nuclease activity of both compounds. Influence of H$_2$O$_2$ is more important than that of singlet oxygen, as pre-exposure to catalase leads to intact pBS (Figure 7C).

3.6 Oxidative stress induced in SK-MEL-147

A flow cytometry assay was used to evaluate the connection between the redox-active nature of copper, and the significative antitumoral activity observed for the hybrid copper materials loaded on the POSS-atzac matrix. The oxidative stress assay is based on the intracellular detection of superoxide by the dihydroethidium probe. Upon oxidation, the highly fluorescent ethidium is formed allowing the distinction between live cells (ROS-) and cells undergoing oxidative stress (ROS+). SK-MEL-147 cells exposed to the free matrices or the matrices loaded with the copper(II) complexes showed an increase in the percentage of the ROS+ populations, indicating that such stimuli trigger the presence of oxidative species in the cells (Figure 8 and S12). Finally, this experiment revealed that the loaded materials containing [Cu(isapn)]$^+$ or [Cu(isaepy)]$^+$ have a similar effect on the intracellular

ROS state in SK-MEL-147 cells to that observed for the free POSS-atzac matrix. This pro-oxidant effect of the free matrix was also observed by the enhanced oxidation of melanin observed in the presence of POSS-atzac.
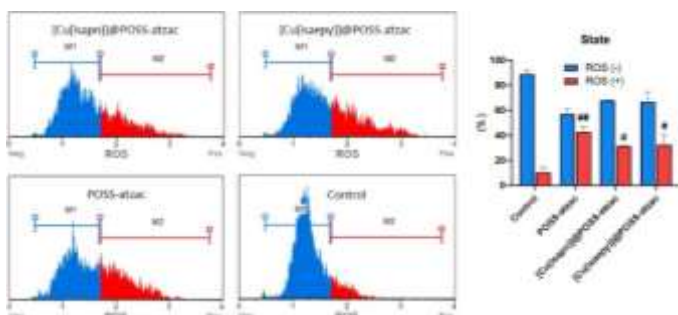

Figure 8. Analysis of the oxidative stress induced on SK-MEL-147 cells upon 24h treatment at IC_{50} concentration of POSS-atzac, [Cu(isapn)]@POSS-atzac and [Cu(isaepy)]@POSS-atzac in comparison to untreated cells (control). The bar graph shows the percentage of cells identified with low intensity (ROS-, marked in blue) or high intensity (ROS+, marked in red) based on the oxidation of dihydroethidium. # significance in relation to the control ROS(+): # 0.05, ## 0.01. Statistical analysis was performed by one-way ANOVA by Tukey post-test.

For comparison, it was showed previously that the free [Cu(isapn)] induced oxidative stress in SH-SY5Y neuroblastoma cells [15]. Intracellular ROS production was determined in a similar assay, based on 2',7'-dichlorodihydrofluorescein diacetate. Cytofluorimetric analyses showed that [Cu(isapn)] was a pro-oxidant, with ROS production increased with respect to untreated cells. [Cu(isapn)) was a potent upstream ROS inducer, with increase of fluorescence detectable as early as 3 h after treatment.

3.7 Melanin oxidation

Melanin synthesis and chemiexcitation are central regulators of melanoma progression and resistance to photodynamic therapy. Melanin itself can exhibit a dual rule being pro- or antioxidant, and thus interfering in cellular redox homeostasis [64]. Their chemical properties include binding to metal ions [65] and crucial molecules as DNA [66], and displaying of redox activity.

Considering the remarkable selectivity for melanoma cells (SK-MEL-147) of the loaded materials that contains binuclear species in addition to corresponding mononuclear ones, the possibility of interactions between these complexes with melanin was explored. Previous studies in our lab reported the higher activity of similar binuclear di-imine-copper(II) complexes when compared to analogous mononuclear species against melanomas [58, 63]. Further, the binuclear complexes show a significant increase in their cytotoxicity by action of UV light, which is not observed with the complexes with a single central copper. Results indicated that cells with higher level of melanin (activated or not by light) are more susceptible to these binuclear copper(II) complexes [63].

For these studies, a fluorescence-based microplate assay was developed to evaluate the oxidation of melanin induced by the compounds of interest under physiological conditions. Melanin samples were exposed to the loaded materials [Cu(isapn)]@POSS and [Cu(isaepy)]@POSS (final concentrations of 2.5 or 25 μg/mL) and the free compounds [Cu(isapn)] and [Cu(isaepy)]$^+$ (final concentrations of 1 or 10 μM). Each compound was assayed in triplicate in PBS 1x pH 7.4, reproducing the physiological conditions used in the cell-based assays and the copper release assays. The compounds were evaluated in the presence of H_2O_2, the oxidizing agent classically used in melanin bleaching experiments [48, 67], and in the presence of ascorbate, in analogy to the conditions used for the nuclease activity assay (section 3.4.1). The time course of the oxidation was followed over 24 h, with 30 min intervals. The results are shown in Figure 9.

Among the loaded materials, [Cu(isaepy)]@POSS had a distinguished behavior. On its own at 25 μg/mL, melanin oxidation (albeit low) can already be observed over time. This effect is even more pronounced in the presence of ascorbate, and the compound further potentiates the strong oxidative effect induced by H_2O_2. Interestingly, in the presence of H_2O_2 the compound [Cu(isapn)]@POSS seems to protect melanin from oxidation (the corresponding oxidation curve appears below that of free melanin), highlighting the dichotomic

nature of copper-containing compounds as either pro- or anti-oxidants in physiological conditions [68, 69].

The free matrix POSS-atzac also seems to affect the oxidation of melanin (Figure S13). No effect is observed for the free matrix in the absence of a reducing agent. However, some oxidation occurs by addition of ascorbate, and even higher level of oxidation can be observed in the presence of H_2O_2.
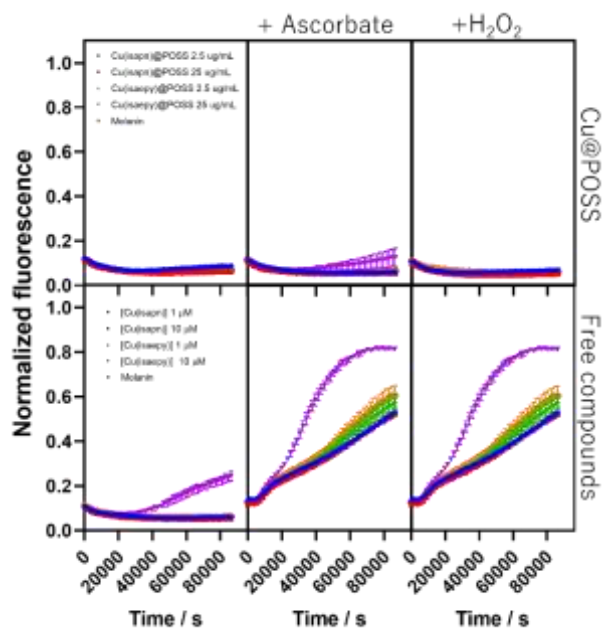

Figure 9. Melanin oxidation assay in PBS 1x pH 7.4, evaluating the loaded materials [Cu(isapn)]@POSS-atzac and [Cu(isaepy)]@POSS-atzac (assayed at 2.5 or 25 µg/mL), in comparison to the free compounds [Cu(isapn)]+ and [Cu(isaepy)]+ (assayed at 1 or 10 µM) The formation of the melanin oxidation product was followed by fluorescence, either in the absence of a Fenton-like reaction starter, or in the presence of ascorbate or H_2O_2.

The free compounds [Cu(isapn)]+ and [Cu(isaepy)}+ had no effect on the oxidation of melanin when assayed either in the absence or in the presence of ascorbate (Figure 9, bottom). However, in the presence of H_2O_2, both complexes [Cu(isapn)]+ and [Cu(isaepy)]+, seem to lead to alternative oxidation pathways. At concentration 1 µM the oxidation curves appear slightly below that of free melanin, during the progress of the reaction, although reaching an identical final endpoint.

At higher concentration (10 µM) both complexes show increased oxidation of melanin in the reaction induced by H_2O_2.

Taken collectively, these experiments demonstrate that the POSS-atzac matrix has a non-passive role in the reactivity of the loaded compounds toward biomolecules. The matrix seems to improve the reactivity of the loaded compounds, mainly by formation of additional binuclear copper species.

Conclusions

In this work, an engineered hexatriazole-substituted polyhedral oligomeric silsesquioxane (POSS-atzac) was synthesized and applied as a drug delivery system for two cytotoxic copper(II) complexes that previously had shown to be efficient against tumor cells.

According to nitrogen elemental analysis of POSS-atzac matrix, six chlorine atoms of the POSS-Cl precursor material were replaced by six 3-amino-1,2,4-triazole-5-carboxylic acid ligands. Additionally, the existence of two different arms ($-CH_2-CH_2-CH_2-Cl$ and $-CH_2-CH_2-CH_2-NR$) was further confirmed by ^{13}C solid-state NMR spectroscopy. The ^{29}Si solid state NMR spectrum of POSS-atzac also confirmed that the Si_8O_{12} core remains intact upon functionalization, as observed by the single ^{29}Si signal.

Continuous-wave EPR spectroscopy of both hybrid materials confirmed the presence of copper(II) complexes on the POSS-atzac surface, interacting magnetically. Further, both loaded materials display a second minor species owing to the dipolar interaction between two copper centers, provided by the flexible atzac arms. This second binuclear minority species are acting as an adjuvant factor to increase the cytotoxicity and selectivity between the loaded matrices and the free complexes or free matrices.

Additional HYSCORE data [43] for [Cu(isapn)]@POSS-atzac was used as a diagnostic for the interaction of a single copper(II) species, surrounded by five nitrogen atoms. Four of them come from the ligand in [Cu(isapn)+ complex, and the fifth nitrogen atom

belongs to the triazole ring of the functionalized-POSS. Therefore, HYSCORE experiments confirmed the coordination of this complex to one of the nitrogen atoms of the triazole ring. The final biological outcome investigated was the cytotoxicity against the melanoma cells SK-MEL-147. The loading of the two copper compounds [Cu(isapn)]$^+$ and [Cu(isaepy)]$^+$ on the POSS-atzac matrix dramatically affected the cytotoxicity of these compounds. Firstly, the cytotoxic potencies were increased. As an example, IC$_{50}$ values expressed in terms of copper molar concentration (μM, 24h incubation) decreased from >100 to 0.66 for [Cu(isapn)]$^+$ and from 38 to 1.76 for [Cu(isaepy)]$^+$. It represents a >150-fold increase for [Cu(isapn)]$^+$. Furthermore, the loading also led to better selectivity indexes, when comparing the IC$_{50}$ against the tumorigenic SK-MEL-147 vs. the non-tumorigenic fibroblast P4. The free POSS-atzac matrix has itself some cytotoxicity against SK-MEL-147, while being non-toxic against the fibroblast P4.

In vitro assays demonstrated the excellent ability of the hybrid materials to promote the oxidative cleavage of plasmidial DNA, with total fragmentation being observed in concentrations as low as 25 μg/mL for both loaded materials. At the same concentration, [Cu(isaepy)]@POSS also exhibits an oxidative activity against melanin, which acts as a resistance factor against chemotherapy in melanoma cells.

A flow cytometry-based assay was used to probe for intracellular oxidative stress. This assay demonstrated that the loaded materials and the free POSS-atzac lead to a statistically significant increase of detectable ROS species in the population of SK-MEL-147 cells after treatment with those materials. This oxidative stress can be assigned both to DNA damage, and to melanin oxidation by interaction with copper species. Therefore, these preliminary results indicate that the preferential mechanism of cytotoxicity of these materials is ROS-dependent.

In this proof-of-concept study, POSS-based materials appear as promising matrices for the drug delivery of cytotoxic metallodrugs, allowing a modulation of the present species. With the desirable increase in cytotoxicity observed for the loaded materials, POSS should receive further attention by the medicinal inorganic chemistry community.

Author Contributions

EGV: conceptualization, data curation, formal analysis, and writing original draft; RBM, APAO, REFP and FFMB: data curation, formal analysis of the biological experiments and writing original draft; CCO: data curation, revised the writing and grammar of the manuscript; FT: designed the advanced EPR experiments, data curation, formal analysis, and revision of the manuscript; AMDCF: conceptualization and supervision of the research, funding acquisition, writing and revision of the manuscript.

All the co-authors have read and approved the final manuscript.

Conflicts of interest

The authors have no conflicts of interest, including competing financial interests or personal relationships, to declare.

The University of São Paulo (USP) and São Paulo State Research Foundation (FAPESP) have a Brazilian patent granted on isatin-derivatives metal complexes based on studies in our laboratory (PI 0600985-9, conceded on March 24th, 2020).

Data availability

The data supporting this article have been included as part of the Supplementary Information. Additional data will be made available on request.

References

1   E. Proksch, J.M. Brandner, and J.-M. Jensen, The skin: an indispensable barrier, *Exp. Dermatol.* 2008, **17**, 1063–1072. doi:10.1111/j.1600-0625.2008.00786.x.

2   J.Y. Lin, and D.E. Fisher, Melanocyte biology and skin pigmentation, *Nature* 2007, **445**, 843–850. doi:10.1038/nature05660.

3   T. Klabunde, C. Eicken, J.C. Sacchettini, B. Krebs, Crystal structure of a plant catechol oxidase containing a dicopper center. *Nat. Struct. Biol.* 1998, **5**, 1084–1090. doi: 10.1038/4193

4   C. Serre, V. Busuttil and J.-M. Botto, Intrinsic and extrinsic regulation of human skin melanogenesis and pigmentation, *Internat. J. Cosmetic Sci.* 2018, **40**, 328–347. doi: 10.1111/ics.12466

5   A. Sánchez-Ferrer, J.N. Rodríguez-López, F. García-Cánovas, F. García-Carmona, Tyrosinase: a comprehensive review of its mechanism, *Biochim. Biophys. Acta*, 1995, **1247**, 1-11. https://doi.org/10.1016/0167-4838(94)00204-T

6   M. Kanteev, M. Goldfeder, and A. Fishman, Structure–function correlations in tyrosinases, *Protein Sci.* 2015, **24**, 1360–1369. doi: 10.1002/pro.2734

7   A. Slominski, T.-K. Kim, A.A. Brożyna, Z. Janjetovic, D.L.P. Brooks, L.P. Schwab, C. Skobowiat, W. Jóźwicki, and T.N. Seagroves, The role of melanogenesis in regulation of melanoma behavior: Melanogenesis leads to stimulation of HIF-1α expression and HIF-dependent attendant pathways, *Arch. Biochem. Biophys.* 2014, **563**, 79–93. doi:10.1016/j.abb.2014.06.030.

8   Y. Yamaguchi, V.J. Hearing, Melanocytes and Their Diseases, *Cold Spring Harb. Perspect. Med.* 2014, **4**, a017046–a017046. doi:10.1101/cshperspect.a017046.

9   M. Cichorek, M. Wachulska, A. Stasiewicz, A. Tymińska, Skin melanocytes: biology and development, *Adv. Dermatology Allergol.* 2013, **1**, 30–41. doi:10.5114/pdia.2013.33376.

10   C. Olivares, F. Solano, New insights into the active site structure and catalytic mechanism of tyrosinase and its related proteins. *Pigm. Cell Melanoma Res.* 2009, **22**, 750–760. doi: 10.1111/j.1755-148X.2009.00636.x

11   GLOBOCAN, WHO, Cancer Today: Melanoma - Global Cancer Observatory, (n.d.). https://gco.iarc.fr/today/data/factsheets/cancers/16-Melanoma-of-skin-fact-sheet.pdf.

12   K.M. Joyce, Surgical Management of Melanoma, in: *Cutan. Melanoma Etiol. Ther.*, Codon Publications, 2017, pp. 91–100. doi:10.15586/codon.cutaneousmelanoma.2017.ch7.

13   A. Gupta, F. Gomes, and P. Lorigan, The role for chemotherapy in the modern management of melanoma, *Melanoma Manag.* 2017, **4**, 125–136. doi:10.2217/mmt-2017-0003

14   G. Cerchiaro, K. Aquilano, G. Filomeni, G. Rotilio, M.R. Ciriolo, A.M.D.C. Ferreira, Isatin-Schiff base copper(II) complexes and their influence on cellular viability., *J. Inorg. Biochem*. 2005, **99**, 1433–40. doi:10.1016/j.jinorgbio.2005.03.013.

15   G. Filomeni, G. Cerchiaro, A.M. Da Costa Ferreira, A. De Martino, J.Z. Pedersen, G. Rotilio, M.R. Ciriolo, Pro-apoptotic activity of novel Isatin-Schiff base copper(II) complexes depends on oxidative stress induction and organelle-selective damage., *J. Biol. Chem.* 2007, **282**,

12010–12021. doi:10.1074/jbc.M610927200.

16   V.C. da Silveira, J.S. Luz, C.C. Oliveira, I. Graziani, M.R. Ciriolo, and A.M. da C. Ferreira, Double-strand DNA cleavage induced by oxindole-Schiff base copper(II) complexes with potential antitumor activity, *J. Inorg. Biochem*. 2008, **102**, 1090–1103. doi:10.1016/j.jinorgbio.2007.12.033.

17   R.E. Ferraz de Paiva, E.G. Vieira, D. Rodrigues da Silva, C.A. Wegermann, A.M. Costa Ferreira, Anticancer Compounds Based on Isatin-Derivatives: Strategies to Ameliorate Selectivity and Efficiency, F*ront. Mol. Biosci.* 2021, **7**, 627272. doi:10.3389/fmolb.2020.627272.

18   R.G. Kenny, and C.J. Marmion, Toward Multi-Targeted Platinum and Ruthenium Drugs—A New Paradigm in Cancer Drug Treatment Regimens? *Chem. Rev*. 2019, **119**, 1058–1137. doi:10.1021/acs.chemrev.8b00271.

19   X. Wang, X. Wang, S. Jin, N. Muhammad, and Z. Guo, Stimuli-Responsive Therapeutic Metallodrugs, *Chem. Rev*. 2019, **119**, 1138–1192. doi:10.1021/acs.chemrev.8b00209.

20   C. Santini, M. Pellei, V. Gandin, M. Porchia, F. Tisato, and C. Marzano, Advances in Copper Complexes as Anticancer Agents, *Chem. Rev*. 2014, **114**, 815–862. doi:10.1021/cr400135x.

21   S.A. Andres, K. Bajaj, N.S. Vishnosky, M.A. Peterson, M.S. Mashuta, R.M. Buchanan, P.J. Bates, and C.A. Grapperhaus, Synthesis, Characterization, and Biological Activity of Hybrid Thiosemicarbazone–Alkylthiocarbamate Metal Complexes, *Inorg. Chem*. 2020, **59**, 4924–4935. doi:10.1021/acs.inorgchem.0c00182.

22   L. Brustolin, C. Nardon, N. Pettenuzzo, N. Zuin Fantoni, S. Quarta, F. Chiara, A. Gambalunga, A. Trevisan, L. Marchiò, P. Pontisso, and D. Fregona, Synthesis, chemical characterization and cancer cell growth-inhibitory activities of Cu(II) and Ru(III) aliphatic and aromatic dithiocarbamato complexes, *Dalton Trans*. 2018, **47**, 15477–15486. doi:10.1039/C8DT02965B.

23   S. Castelli, M. B. Gonçalves, P. Katkar, G. C. Stuchi, R. A. A. Couto, H. M. Petrilli, A. M. da Costa Ferreira, Comparative studies of oxindolimine-metal complexes as inhibitors of human DNA topoisomerase IB. *J. Inorg. Biochem.* 2018, **186**, 85-94. https://doi.org/10.1016/j.jinorgbio.2018.05.012

24   E. Guimarães Vieira, R.B. Miguel, D. Rodrigues da Silva, R. Boni Fazzi, R.A.A. de Couto, J.H. Marin, M.L.A. Temperini, J. da Silva Shinohara, H.E. Toma, L.C. Russo, Y.T. Magalhães, N.L. Dias Filho, F.L. Forti, and A.M. da Costa Ferreira, Functionalized nanoparticles as adjuvant to increase the cytotoxicity of metallodrugs toward tumor cells, *New J. Chem*. 2019, **43**, 386–398. doi:10.1039/C8NJ04654A.

25   C. He, D. Liu, W. Lin, Nanomedicine Applications of Hybrid Nanomaterials Built from Metal–Ligand Coordination Bonds: Nanoscale Metal–Organic Frameworks and Nanoscale Coordination Polymers, *Chem. Rev*. 2015, **115**, 11079–11108. doi:10.1021/acs.chemrev.5b00125.

26   H. Chen, D. Liu, Z. Guo, Endogenous Stimuli-responsive Nanocarriers for Drug Delivery, *Chem. Lett.* 2016, **45**, 242–249. doi:10.1246/cl.151176.

27   Xin Du, Xiaoyu Li, Lin Xiong, Xueji Zhang, Freddy Kleitz, Shi Zhang Qiao, Mesoporous silica nanoparticles with organo-bridged silsesquioxane framework as innovative platforms for bioimaging and therapeutic agent delivery, *Biomaterials* 2016, **91**, 90-127

28   D. Tarn, M. Xue, and J.I. Zink, pH-Responsive Dual Cargo Delivery from Mesoporous Silica Nanoparticles with a Metal-Latched Nanogate,

Inorg. Chem. 2013, **52**, 2044–2049. doi:10.1021/ic3024265.

29   S. Liu, R. Guo, C. Li, C. Lu, G. Yang, F. Wang, J. Nie, C. Ma, M. Gao, POSS hybrid hydrogels: A brief review of synthesis, properties and applications, *Eur. Polym. J.* 2021, **143**, 110180. doi:10.1016/j.eurpolymj.2020.110180.

30   I. V. Soares, E.G. Vieira, N.L.D. Filho, A.C. Bastos, N.C. da Silva, E.F. Garcia, L.J.A. Lima, Adsorption of heavy metal ions and epoxidation catalysis using a new polyhedral oligomeric silsesquioxane, *Chem. Eng. J.* 2013, **218**, 405–414. doi:10.1016/j.cej.2012.11.126.

31   A. Noureddine, and C. J. Brinker, Pendant/bridged/mesoporous silsesquioxane nanoparticles: Versatile and biocompatible platforms for smart delivery of therapeutics, *Chem. Eng. J.* 2018, **340**, 125–147. doi:10.1016/j.cej.2018.01.086.

32   B.P. Nair, D. Vaikkath, and P.D. Nair, Polyhedral Oligomeric Silsesquioxane-F68 Hybrid Vesicles for Folate Receptor Targeted Anti-Cancer Drug Delivery, *Langmuir* 2014, **30**, 340–347. doi:10.1021/la4036997.

33   M.J. Sailor, J.-H. Park, Hybrid Nanoparticles for Detection and Treatment of Cancer, *Adv. Mater*. 2012, **24**, 3779–3802. doi:10.1002/adma.201200653.

34   D. Dheer, V. Singh, R. Shankar, Medicinal attributes of 1,2,3-triazoles: Current developments, *Bioorg. Chem*. 2017, **71**, 30–54. doi:10.1016/J.BIOORG.2017.01.010.

35   Ş.G. Küçükgüzel, and P. Çıkla-Süzgün, Recent advances bioactive 1,2,4-triazole-3-thiones, *Eur. J. Med. Chem.* 2015, **97**, 830–870. doi:10.1016/j.ejmech.2014.11.033.

36   N. Nehra, R.K. Tittal, V.D. Ghule, 1,2,3-Triazoles of 8-Hydroxyquinoline and HBT: Synthesis and Studies (DNA Binding, Antimicrobial, Molecular

Docking, ADME, and DFT), *ACS Omega* 2021, **6**, 27089–27100. doi:10.1021/acsomega.1c03668.

37   S.H. Sumrra, W. Zafar, M.L. Asghar, F. Mushtaq, M.A. Raza, M.F. Nazar, M.A. Nadeem, M. Imran, and S. Mumtaz, Computational investigation of molecular structures, spectroscopic properties, cholinesterase inhibition and antibacterial activities of triazole Schiff bases endowed metal chelates, *J. Mol. Struct.* 2021, **1238**, 130382. doi:10.1016/j.molstruc.2021.130382.

38   O.R. Hordiichuk, Y.I. Slyvka, V. V. Kinzhybalo, E.A. Goreshnik, T.J. Bednarchuk, O. Bednarchuk, J. Jedryka, I. Kityk, and M.G. Mys'kiv, Construction of heterometallic and mixed-valence copper(I/II) chloride π-complexes with 1,2,4-triazole allyl-derivative, *Inorganica Chim. Acta* 2019, **495**, 119012. doi:10.1016/j.ica.2019.119012.

39   K. Piorecka, A. Janaszewska, M. Majkowska, M. Marcinkowska, J. Kurjata, S. Kazmierski, E. Radzikowska-Cieciura, B. Kost, P. Sowinski, B. Klajnert-Maculewicz, and W.A. Stanczyk, Hydrophilic Polyhedral Oligomeric Silsesquioxane, POSS(OH)32, as a Complexing Nanocarrier for Doxorubicin and Daunorubicin, *Materials* (Basel). 2020, **13**, 5512. doi:10.3390/ma13235512.

40   J. Zhang, Z. Luo, W. Wang, Y. Yang, D. Li, and Y. Ma, One-pot synthesis of bio-functionally water-soluble POSS derivatives via efficient click chemistry methodology, *React. Funct. Polym.* 2019, **140**, 103–110. doi:10.1016/j.reactfunctpolym.2019.04.013.

41   Y.-X. Zhu, H.-R. Jia, Z. Chen, and F.-G. Wu, Photosensitizer (PS)/polyhedral oligomeric silsesquioxane (POSS)-crosslinked nanohybrids for enhanced imaging-guided photodynamic cancer therapy, *Nanoscale* 2017, **9**, 12874–12884. doi:10.1039/C7NR02279D.

42   G. Filomeni, S. Piccirillo, I. Graziani, S. Cardaci,

A.M. Da Costa Ferreira, G. Rotilio, M.R. Ciriolo, The isatin-Schiff base copper(II) complex Cu(isaepy) 2 acts as delocalized lipophilic cation, yields widespread mitochondrial oxidative damage and induces AMP-activated protein kinase-dependent apoptosis, *Carcinogenesis* 2009, **30**, 1115–1124. doi:10.1093/carcin/bgp105.

43 E. G. Vieira, R. B. Fazzi, D. O. T. A. Martins, A. M. Sheveleva, F. Tuna, A. M. da Costa Ferreira, A new strategy of improving cytotoxicity of copper complex toward metastatic melanoma cells unveiled by EPR spectroscopy. *RSC, Advances* 2023, **13**, 9715–9719. doi: 10.1039/d2ra07266a.

44 S. Stoll, and A. Schweiger, EasySpin, a comprehensive software package for spectral simulation and analysis in EPR, *J. Magn. Reson*. 2006, **178**, 42–55. doi:10.1016/j.jmr.2005.08.013.

45 G. Cerchiaro, G.A. Micke, M.F.M. Tavares, A.M. da Costa Ferreira, Kinetic studies of carbohydrate oxidation catalyzed by novel isatin-Schiff base copper(II) complexes, *J. Mol. Catal. A Chem.* 2004, **221**, 29–39. doi:10.1016/j.molcata.2004.06.017.

46 E.G. Vieira, I. V. Soares, G. Pires, R.A.V. Ramos, D.R. do Carmo, and N.L. Dias Filho, Study on determination and removal of metallic ions from aqueous and alcoholic solutions using a new POSS adsorbent, *Chem. Eng. J.* 2015, **264**, 77–88. doi:10.1016/j.cej.2014.11.050.

47 E.G. Vieira, A.G. Dal-Bó, T.E.A. Frizon, and N.L. Dias Filho, Synthesis of two new Mo(II) organometallic catalysts immobilized on POSS for application in olefin oxidation reactions, *J. Organomet. Chem.* 2017, **834**, 73–82. doi:10.1016/j.jorganchem.2017.02.010.

48 W. Korytowski, and T. Sarna, Bleaching of melanin pigments. Role of copper ions and hydrogen peroxide in autooxidation and

photooxidation of synthetic dopa-melanin., *J. Biol. Chem.* 1990, **265**, 12410–6. doi:2165063.

49 E.G. Vieira, R.O. Silva, E.F. Junior, and N.L. Dias Filho, Synthesis, characterization and catalytic application of a new organometallic oligomer based on polyhedral oligomeric silsesquioxane, *Appl. Organomet. Chem*. 2017, **31**, e3722. doi:10.1002/aoc.3722.

50 F. Ciesielczyk, K. Szwarc-Rzepka, M. Przybysz, J. Czech-Polak, M. Heneczkowski, M. Oleksy, and T. Jesionowski, Comprehensive characteristic and potential application of POSS-coated MgO-SiO2 binary oxide system, *Colloids Surfaces A Physicochem. Eng. Asp.* 2018, **537**, 557–565. doi:10.1016/j.colsurfa.2017.10.005.

51 N. Liang, Y. Tu, J. Xu, D. Chen, and H. Zhang, Hybrid anion exchange membranes with self-assembled ionic channels, *Adv. Polym. Technol.* 2018, **37**, 1732–1736. doi:10.1002/adv.21831.

52 W. Li, H.P. Jia, Z.F. Ju, J. Zhang, A novel chiral Cd(II) coordination polymer based on achiral unsymmetrical 3-amino-1,2,4-triazole with an unprecedented μ4-bridging mode, *Cryst. Growth Des.* 2006, **6**, 2136–2140. doi:10.1021/cg060363w.

53 C. Ramírez, M. Rico, A. Torres, L. Barral, J. López, B. Montero, Epoxy/POSS organic–inorganic hybrids: ATR-FTIR and DSC studies, *Eur. Polym. J.* 2008, **44**, 3035–3045. doi:10.1016/j.eurpolymj.2008.07.024.

54 J. Bai, Y. Zhang, W. Zhang, X. Ma, Y. Zhu, X. Zhao, Y. Fu, Synthesis and characterization of molecularly imprinted polymer microspheres functionalized with POSS, Appl. Surf. Sci. 511 (2020) 145506. doi:10.1016/j.apsusc.2020.145506.

55 Y. Niu, R. Qu, H. Chen, L. Mu, X. Liu, T. Wang, Y. Zhang, C. Sun, Synthesis of silica gel supported salicylaldehyde modified PAMAM dendrimers for the effective removal of Hg(II) from aqueous

solution, *J. Hazard. Mater*. 2014, **278**, 267–278. doi:10.1016/j.jhazmat.2014.06.012.

56 E.G. Vieira, R.O. Silva, A.G. Dal-Bó, T.E.A. Frizon, N.L.D. Filho, Syntheses and catalytic activities of new metallodendritic catalysts, *New J. Chem*. 2016, **40**, 9403–9414. doi:10.1039/C6NJ01629D.

57 P.M. Dias, L. Kinouti, V.R.L. Constantino, A.M. da Costa Ferreira, M.B. Gonçalves, R.R. Do Nascimento, H.M. Petrilli, M. Caldas, R.C.G. Frem, Spectroscopic characterization of Schiff base-copper complexes immobilized in smectite clays, *Quim. Nova* 2010, **33**, 2135–2142. doi:10.1590/S0100-40422010001000025.

58 C.J. Nunes, B.E. Borges, L.S. Nakao, E. Peyroux, R. Hardré, B. Faure, M. Réglier, M. Giorgi, M.B. Prieto, C.C. Oliveira, and A.M. Da Costa Ferreira, Reactivity of dinuclear copper(II) complexes towards melanoma cells: Correlation with its stability, tyrosinase mimicking and nuclease activity, *J. Inorg. Biochem*. 2015, **149**, 49–58. doi:10.1016/j.jinorgbio.2015.05.007.

59 L.-P. Zhang, S.-H. Tang, C.-E. Mo, C. Wang, Y.-P. Huang, Z.-S. Liu, Synergistic effect of liquid crystal and polyhedral oligomeric silsesquioxane to prepare molecularly imprinted polymer for paclitaxel delivery, *Eur. Polym. J.* 2018, **98**, 226–236. doi:10.1016/j.eurpolymj.2017.11.021.

60 V. Mamaeva, C. Sahlgren, M. Lindén, Mesoporous silica nanoparticles in medicine—Recent advances, *Adv. Drug Deliv. Rev.* 2013, **65**, 689–702. doi:10.1016/j.addr.2012.07.018.

61 Y. Li, S. Wang, F.X. Song, L. Zhang, W. Yang, H.X. Wang, Q.L. Chen, A pH-sensitive drug delivery system based on folic acid-targeted HBP-modified mesoporous silica nanoparticles for cancer therapy, *Colloids Surfaces A Physicochem. Eng. Asp*. 2020, **590**, 124470. doi:10.1016/j.colsurfa.2020.124470.

62 R.R. Massaro, F. Faião-Flores, V.W. Rebecca, S. Sandri, D.K. Alves-Fernandes, P.C. Pennacchi, K.S.M. Smalley, S.S. Maria-Engler, Inhibition of proliferation and invasion in 2D and 3D models by 2-methoxyestradiol in human melanoma cells, *Pharmacol. Res.* 2017, **119**, 242–250. doi:10.1016/j.phrs.2017.02.013.

63 C.J. Nunes, A.H. Otake, S.O. Bustos, R.B. Fazzi, R. Chammas, A.M. Da Costa Ferreira, Unlike reactivity of mono- and binuclear imine-copper(II) complexes toward melanoma cells via a tyrosinase-dependent mechanism, *Chem. Biol. Interact.* 2019, **311**, 108789. doi:10.1016/j.cbi.2019.108789.

64 A.A. Suzukawa, A. Vieira, S.M.B. Winnischofer, A.C. Scalfo, P. Di Mascio, A.M. da Costa Ferreira, J.-L. Ravanat, D. de L. Martins, M.E.M. Rocha, and G.R. Martinez, Novel properties of melanins include promotion of DNA strand breaks, impairment of repair, and reduced ability to damage DNA after quenching of singlet oxygen, *Free Radic. Biol. Med.* 2012, **52**, 1945–1953. doi:10.1016/j.freeradbiomed.2012.02.039.

65 P.J. Farmer, S. Gidanian, B. Shahandeh, A.J. Di Bilio, N. Tohidian, F. L. Meyskens, Melanin as a Target for Melanoma Chemotherapy: Pro-oxidant Effect of Oxygen and Metals on Melanoma Viability, *Pigment Cell Res.* 2003, **16**, 273–279. doi:10.1034/j.16000749.2003.00046.x.

66 J. Geng, P. Yuan, C. Shao, S.-B. Yu, B. Zhou, P. Zhou, X.-D. Chen, Bacterial melanin interacts with double-stranded DNA with high affinity and may inhibit cell metabolism in vivo, *Arch. Microbiol.* 2010, **192**, 321–329. doi:10.1007/s00203-010-0560-1.

67 J.-Y. Chung, J. Choi, J.D. Sears, K. Ylaya, C. Perry, C.H. Choi, S.-M. Hong, H. Cho, K.M. Brown, and S.M. Hewitt, A melanin-bleaching methodology for molecular and histopathological analysis of formalin-fixed paraffin-embedded tissue, *Lab. Investig.* 2016, **96**, 1116–1127.

doi:10.1038/labinvest.2016.90.

68   M. Bagnati, C. Perugini, C. Cau, R. Bordone, E. Albano, and G. Bellomo, When and why a water-soluble antioxidant becomes pro-oxidant during copper-induced low-density lipoprotein oxidation: a study using uric acid., *Biochem. J.* 1999, **340**, 143–52. doi:10229669.

69   S. Srivastava, P.J. Blower, A.A. Aubdool, R.C. Hider, G.E. Mann, and R.C. Siow, Cardioprotective effects of Cu(II)ATSM in human vascular smooth muscle cells and cardiomyocytes mediated by Nrf2 and DJ-1, *Sci. Rep.* 2016, **6**, 7. doi:10.1038/s41598-016-0012-5.